

Supporting Information for

High energy density Na-metal battery enabled by a tailored carbonate-based electrolyte

Jiawei Chen,^a Yu Peng,^a Yue Yin,^a Mingzhu Liu,^b Zhong Fang,^a Yihua Xie,^a Bowen Chen,^c Yongjie Cao,^a Lidan

Xing,^b Jianhang Huang,^a Yonggang Wang,^a Xiaoli Dong^{*a} and Yongyao Xia^{*a}

- a. Department of Chemistry and Shanghai Key Laboratory of Molecular Catalysis and Innovative Materials, Institute of New Energy, iChEM (Collaborative Innovation Center of Chemistry for Energy Materials), Fudan University, Shanghai 200433, China. E-mail: xldong@fudan.edu.cn; yyxia@fudan.edu.cn
- b. National and Local Joint Engineering Research Center of MPTES in High Energy and Safety LIBs, Engineering Research Center of MTEES (Ministry of Education), Research Center of BMET (Guangdong Province), Key Lab. of ETESPG (GHEI), Innovative Platform for ITBMD (Guangzhou Municipality), School of Chemistry, South China Normal University, Guangzhou 510006, China
- c. i-Lab, CAS Center for Excellence in Nanoscience, Suzhou Institute of Nano-Tech and Nano-Bionics (SINANO), Chinese Academy of Sciences (CAS), Suzhou 215123, China

Experimental section

Density function theory (DFT) calculations

DFT calculations were performed on Gaussian 09 software package. The molecular geometrical configurations were optimized at the B3LYP/6-311++G(d) level. The simulation of liquid environment was considered by using the continuous polarization medium model (PCM) method with the dielectric constant of acetone. Frequency analyses were done at the same level to confirm the obtained optimized stationary point.

Molecular dynamics (MD) simulations

Molecular dynamics (MD) simulation investigations on F/D (1/1) + 0.5% LiDFBOP were proceeded with Forcite module in Material Studio software. The COMPASSII force field was chosen for all the molecular dynamic simulations and the time step was fixed at 1.0 fs (femtosecond). The system was experienced at least 20 ps (picosecond) equilibration steps in the NVT ensemble. After equilibration steps, the production runs were carried in an NPT ensemble of 200 ps with using the Berendsen barostat to maintain 0.1 GPa pressure with 0.1 ps decay constant. All the steps were conducted in a Nosé thermostat with target temperatures of 298K. The simulation time was long enough to ensure the electrolyte system in equilibrium.

Preparations of electrolytes, electrodes, and cells

Cell-grade sodium hexafluorophosphate (NaPF_6), fluoroethylene carbonate (FEC), diethyl carbonate (DEC), 1 M NaPF_6 in 1,2-dimethoxyethane (DME) and 1 M NaPF_6 in ethylene carbonate (EC)/propylene carbonate (PC) (1/1 by volume) electrolytes were purchased from DodoChem Co., Ltd. (China), while lithium difluorobis(oxalato) phosphate (LiDFBOP, 98.7%) was provided by Shanghai Rolechem Co., Ltd. (China). Prior to preparations of electrolytes, solvents were dried by 4\AA zeolites to make sure the water content was lower than 10 ppm, which was tested by 831 KF Coulometer (Metrohm, Switzerland). All preparations were carried out

within an Ar-filled glove box (MIKROUNA, China), where the contents of both O₂ and H₂O are below 0.1 ppm.

A slurry consisting of 85 wt.% artificial graphite (AG, Shanshan Co., Ltd., China), 10 wt.% super P as well as 5 wt.% sodium alginate (SA) in deionized water was coated on Cu current collector, followed by being dried under vacuum at 80°C for 12 h and punched into disks of 1.13 cm², to obtain AG electrodes having an average active material mass loading of 0.8 mg cm⁻². To prepare Na₃V₂(PO₄)₂F₃ cathodes, 90 wt.% Na₃V₂(PO₄)₂F₃ (Shenzhen Kejing Star Technology Co., Ltd., China), 5 wt.% super P, and 5 wt.% polyvinylidene fluoride (PVdF) were mixed in N-methylpyrrolidone (NMP) to form a slurry, which was then coated on Al current collector and dried under vacuum at 120°C for 12 h and punched into disks of 1.13 cm². The typical mass load of Na₃V₂(PO₄)₂F₃ was around 6 mg cm⁻².

For coin cell configurations, each CR-2016 type coin cell was fabricated using Celgard2400 (America) as the separator with 60 μL electrolyte. In order to eliminate the interference (in terms of electrode polarization and stability) from Na metal that was severed as both counter electrode and reference electrode in two-electrode system, some specific cases (including the electrochemical tests in Fig. 5d, S5, S9, S19 and S22) utilized a special three-electrode device,¹ where two Na foils were used as reference electrode and counter electrode respectively, and around 300μL of electrolyte should be added. For pouch cell configurations, aforesaid Na₃V₂(PO₄)₂F₃ and AG electrodes were cut into rectangles with the size of 26.7 cm² and 27.0 cm² respectively. After depositing a certain amount of Na on AG electrode as anode, Na₃V₂(PO₄)₂F₃ cathode was then combined with as-prepared anode and Celgard2400, together with 500 μL electrolyte, to assemble full cell in a pouch format. All cells configurations were conducted in the glove box mentioned above.

Electrochemical measurements

Linear sweep voltammetry (LSV), cyclic voltammetry (CV), and chronoamperometry (CA) measurements were conducted on VMP3 potentiostats (BioLogic, France). Electrochemical impedance spectroscopy (EIS)

measurement was carried out on PGSTAT-30 electrochemical station (Metrohm, Switzerland) with amplitude of 10 mV over a frequency range of 10^5 Hz to 0.01 Hz. The cycling tests and rate capabilities of cells were all tested on a standard battery tester (CT4008, Neware, China). AG electrode was used as the substrate for Na deposition in this work unless otherwise stated, since several recent papers had reported the advantages of graphitic electrode as Na host.^{2,3} For cycling performance of Na plating/stripping CE, 1 mAh cm⁻² of Na was deposited on the AG substrate at a current density of 0.5 mA cm⁻² followed by stripping to 1 V, after 10 cycles of SEI formation at 0.1 mA cm⁻² between 0 V to 1 V. For the Adams CE test,⁴ a standard protocol was followed: 1) performed one initial formation cycle with Na deposition of 5 mAh cm⁻² on AG substrate under 0.5 mA cm⁻² and stripping to 1 V; 2) deposited 5 mAh cm⁻² Na on AG substrate under 0.5 mA cm⁻² as a Na reservoir (the corresponding capacity (5 mAh cm⁻²) was denoted as $Q_{reservoir}$); 3) repeatedly stripped/plated Na of 1 mAh cm⁻² under 0.5 mA cm⁻² for 10 cycles; 4) stripped all residual Na to 1 V (the corresponding capacity was denoted as $Q_{residual}$). The average CE was calculated by dividing the total stripping capacity by the total plating capacity after the initial formation cycle based on the following equation:

$$CE = \frac{n \times Q_{cycle,strip} + Q_{residual}}{n \times Q_{cycle,plate} + Q_{reservoir}}$$

where n is the cycle number (10 cycles in this work) at the charge capacity of $Q_{cycle,strip}$ and discharge capacity of $Q_{cycle,plate}$ (both were 1 mAh cm⁻² in this work). For calendar ageing test, after 10 cycles normal Na plating/stripping on AG at 0.5 mA cm⁻² and 1 mAh cm⁻², additional procedure was introduced every other cycle, which was that the cell was aged for a period of time (10 h, 24 h, 48 h and a week) after deposited 1 mAh cm⁻² Na. For conventional Na||Na symmetric cells cycling tests, 1 mAh cm⁻² of Na was repeatedly stripped/plated with the current density of 1 mA cm⁻². For harsh Na||Na@AG quasi-symmetric cells cycling tests at a Na utilization of 20%, a standard protocol was followed: 1) performed one initial formation cycle with Na deposition of 5 mAh cm⁻² on AG substrate under 0.5 mA cm⁻² and stripping to 1 V; 2) deposited 5 mAh cm⁻² Na on AG substrate under 0.5 mA cm⁻² as a Na reservoir; 3) repeatedly stripped/plated Na of 1 mAh cm⁻² under 0.5

mA cm⁻². The cycling performance of Na||Na₃V₂(PO₄)₂F₃ half cell and Na||Na₃V₂(PO₄)₂F₃ full cell (Na-metal anode in full cell was prepared by plating a certain amount of Na on AG substrate) was obtained at 1 C (1 C = 128 mA g⁻¹) in the voltage range of 2-4.5 V. The electrochemical performance at different temperatures was carried out within an RGD-100 constant temperature and humidity chamber (Wuxi City Su Rui Experimental Equipment Co., Ltd, China). Prior to tests, all cells were maintained at specified temperature for 2 h.

Material characterizations

Scanning electron microscope (SEM) images were obtained on Hitachi S4800 (Hitachi, Japan) with the accelerating voltage of 5 kV. Transmission electron microscope (TEM) analysis was performed on Tecnai G2 F20 S-Twin (FEI, America) with the accelerating voltage of 200 kV. Atomic force microscopy (AFM) measurements were carried out on a Cypher S AFM (Asylum Research, Oxford Instruments, Britain) using Si-based probes (AC160TS-R3, Olympus, Japan) with $k \sim 20 \text{ N m}^{-1}$. To investigate the behavior divergence of Na deposition, in-situ optical observations were carried out on an optical microscope (PSM-1000, Motic (Xiamen) Electric Group Co., Ltd., China) using Cu as working electrode. Cu was selected as working electrode for its obvious brightness change after Na plating. The in-situ cells used for the observations could be found in our previous work.⁵ To analyze the chemical compositions of solid electrolyte interphase (SEI) and cathode-electrolyte-interphase (CEI), X-ray photoelectron spectroscopy (XPS) conducted on Nexsa (Thermo fisher Scientific, America) with a monochromatic Al K α X-ray source (excitation energy = 1468.6 eV) was used, accompanied with depth profiling which was obtained by Ar⁺ sputtering at 1 kV for 0, 25, 50 and 75 s. Prior to morphology and composition characterizations, all the retrieved electrodes were washed with DME for three times to remove the residual electrolyte, and then followed by drying for 12 hours under room temperature. The ionic conductivities of electrolytes at different temperatures were calculated via electrochemical impedance spectroscopy (EIS) measurements using two stainless steel sheets (1 cm²) symmetrically placed in the

electrolytes. The ionic conductivities were calculated according to the equation:

$$\sigma = \frac{L}{A \times R}$$

where σ is the calculated ionic conductivity of the electrolyte (S cm^{-1}), L is the fixed distance between the two stainless steel sheets (1 cm), A is the area of stainless steel sheet (1 cm^2), and R refers to the obtained resistance (Ohm).

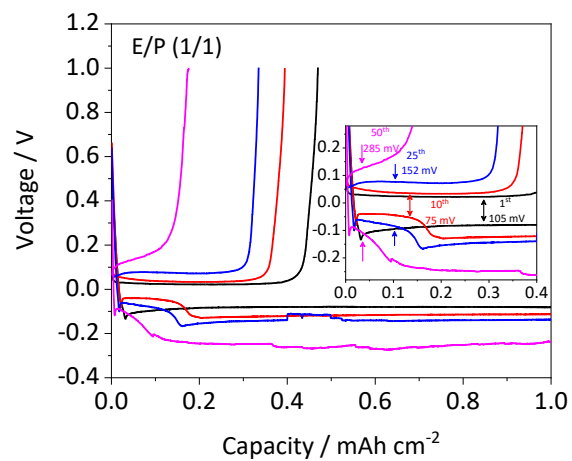


Fig. S1 Galvanostatic plating/stripping voltage profiles of Na on AG performed in E/P (1/1) at 0.5 mA cm⁻² and 1 mAh cm⁻².

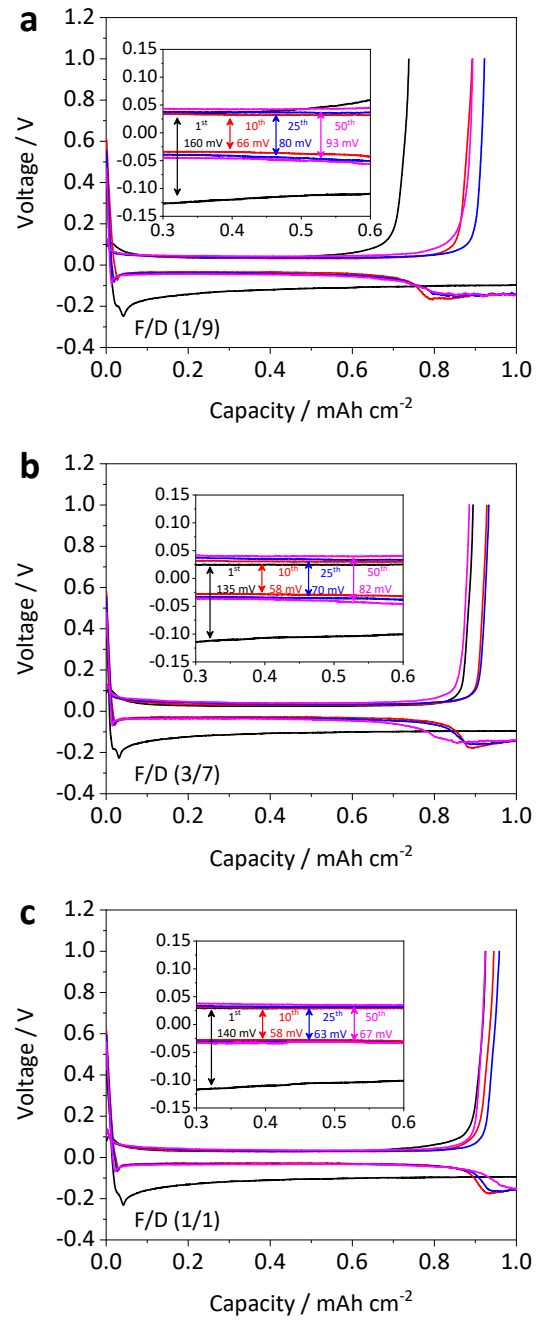


Fig. S2 Galvanostatic plating/stripping voltage profiles of Na on AG performed in (a) F/D (1/9), (b) F/D (3/7) and (c) F/D (1/1) at 0.5 mA cm^{-2} and 1 mAh cm^{-2} .

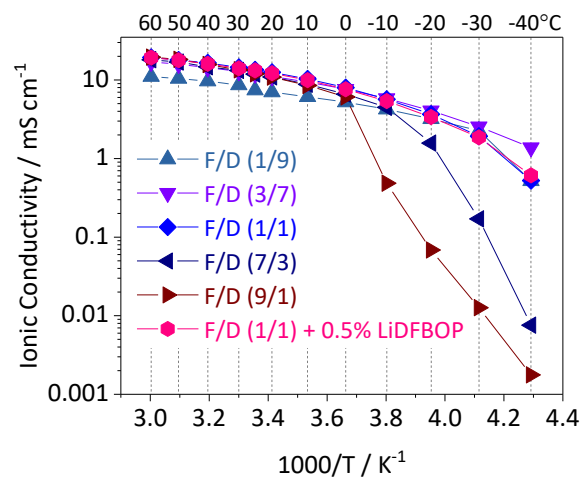


Fig. S3 Temperature-dependent ionic conductivities of various electrolytes.

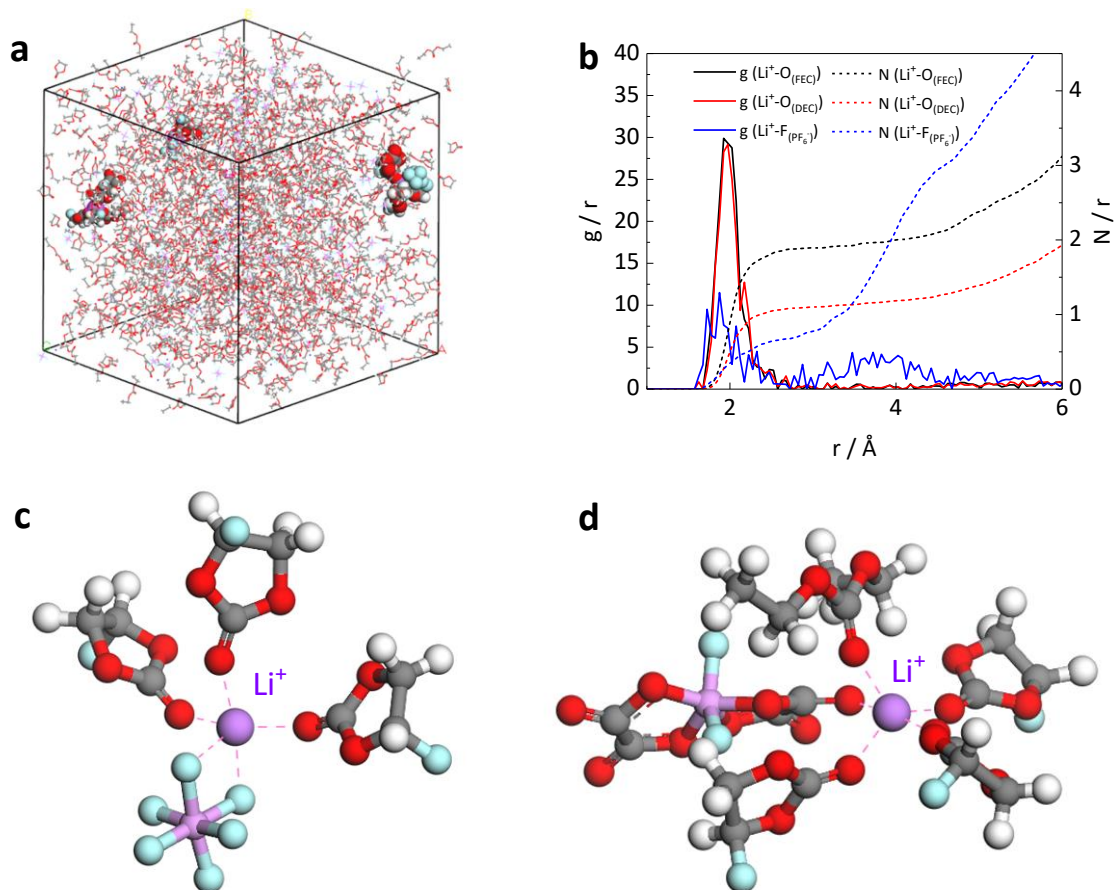


Fig. S4 (a) MD simulated electrolyte structure for F/D (1/1) + 0.5% LiDFBOP. Li^+ and coordinated molecules (within 3 Å of Li^+) are depicted by the CPK (Corey-Pauling-Koltun) model. (b) The radial distribution function ($g(r)$, solid lines) and coordination numbers ($N(r)$, dash lines) for F/D (1/1) + 0.5% LiDFBOP. (c, d) Representative Li^+ solvation structures extracted from the MD simulation.

Fig. S4 displays the radial distribution function and coordination number results. It can be detected that the introduced Li^+ cations will actively participate in solvation structure by coordinating with solvents and anions in the electrolyte. The representative solvation sheath is dominated by FEC, where other basic electrolyte components such as DEC and PF_6^- can also be coordinated by Li^+ .

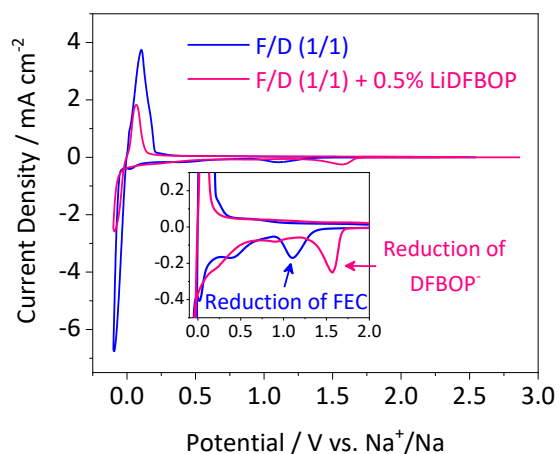


Fig. S5 CV curves of Na plating/stripping on AG operated with F/D (1/1) and F/D (1/1) + 0.5% LiDFBOP in three-electrode devices at a scan rate of 0.5 mV s^{-1} .

The reduction peak at around $1.6 \text{ V vs. Na}^+/\text{Na}$ corresponds to the reduction of DFBOP^- , while the one at around $1.1 \text{ V vs. Na}^+/\text{Na}$ corresponds to the reduction of FEC. It is obvious that the irreversible reduction peak of DFBOP^- is larger than that of FEC, which is indicative of lower CE in the case with LiDFBOP.

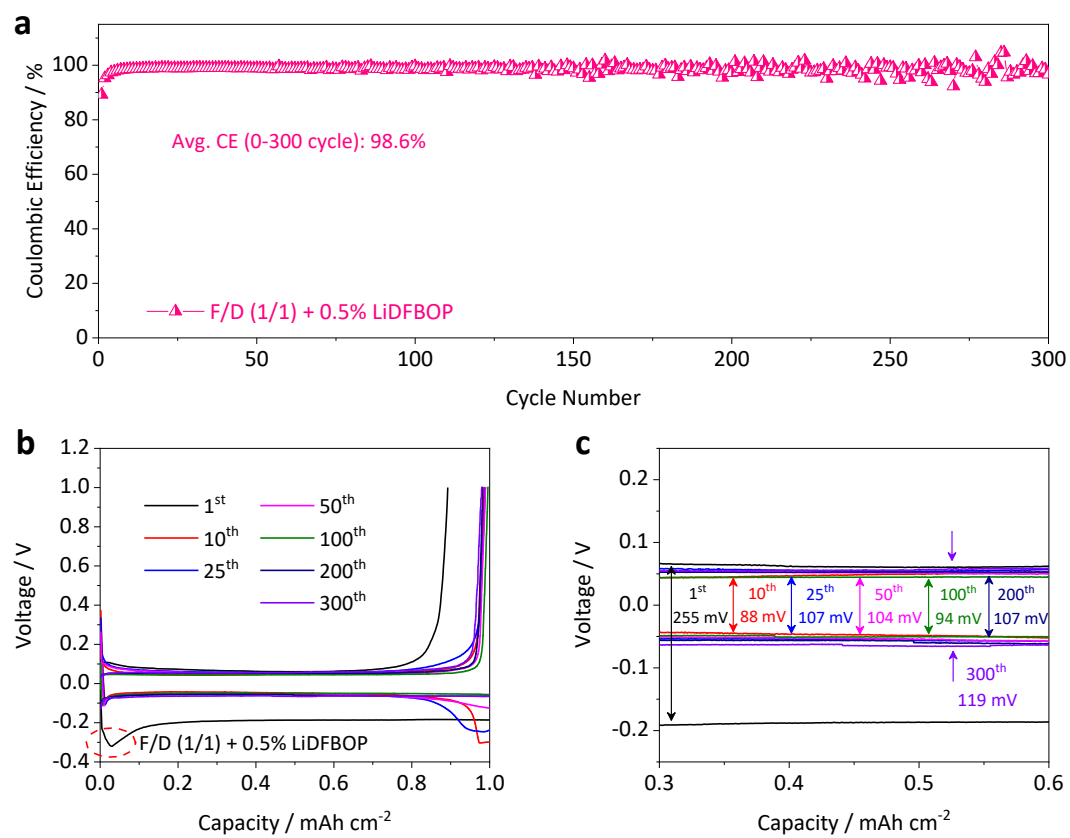


Fig. S6 (a) Long-term cycling tests of Na plating/stripping CE on the AG substrate performed in F/D (1/1) + 0.5% LiDFBOP at 0.5 mA cm⁻² and 1 mAh cm⁻², and corresponding (b) voltage profiles and (c) overpotentials.

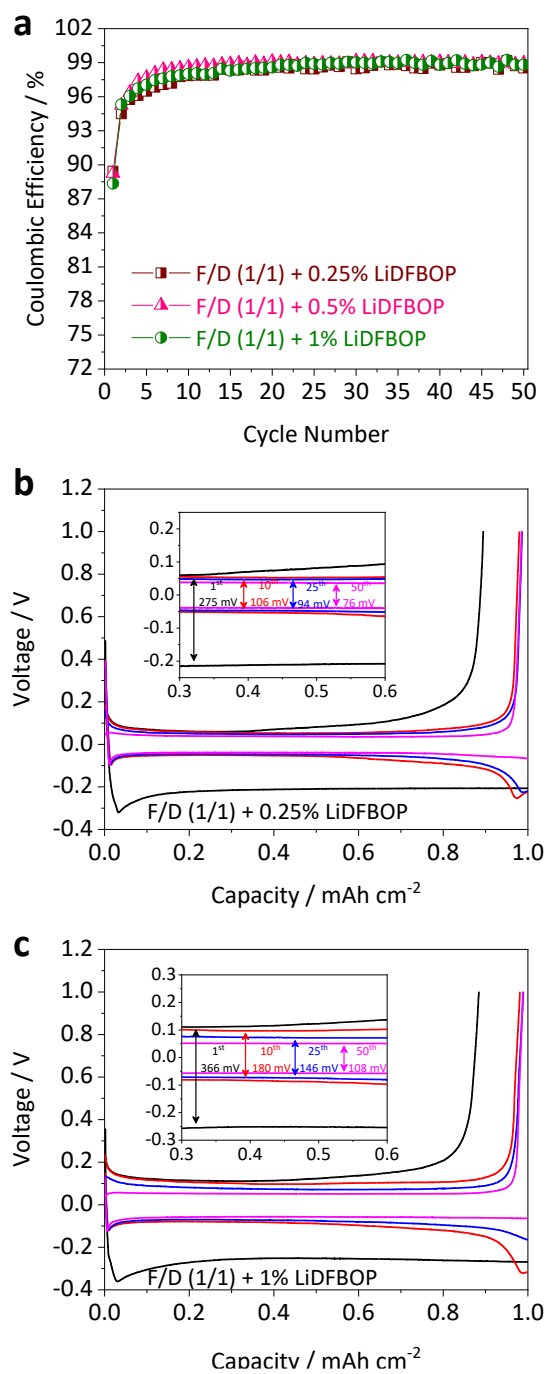


Fig. S7 (a) Cycling tests of Na plating/stripping CE on the AG substrate performed in F/D (1/1) + various contents of LiDFBOP at 0.5 mA cm⁻² and 1 mAh cm⁻², and corresponding voltage profiles in (b) F/D (1/1) + 0.25% LiDFBOP and (c) F/D (1/1) + 1% LiDFBOP.

It can be seen that F/D (1/1) + 0.5% LiDFBOP offers the highest average CE within 50 cycles. Moreover, there is a marked increase in polarization while more amounts of LiDFBOP are added.

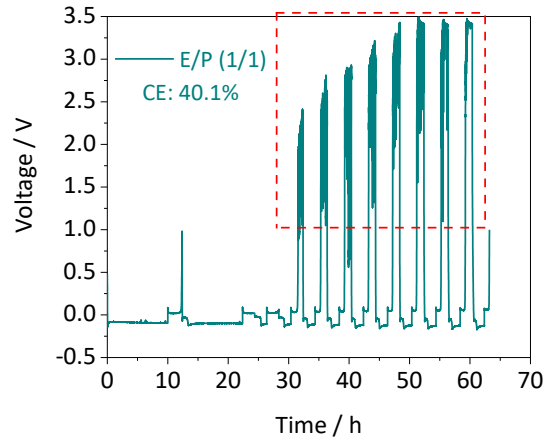


Fig. S8 Adams CE test for Na plating/stripping in E/P (1/1).

When the stripping voltage is higher than 1 V (red frame), it reveals the depletion of available Na sources. Therefore, CE is calculated using the real capacity below 1 V.

$$CE = \frac{Q_{1^{st},strip} + Q_{2^{nd},strip} + \dots + Q_{10^{th},strip} + Q_{residual}}{n \times Q_{cycle,plate} + Q_{reservoir}}$$

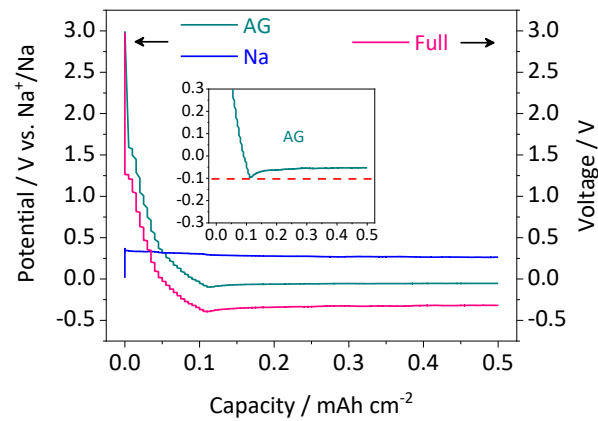


Fig. S9 In-situ monitoring of Na||AG full cell during the first Na plating process in F/D (1/1) + 0.5% LiDFBOP at 0.5 mA cm^{-2} and 0.5 mAh cm^{-2} with a three-electrode device.

The potential profile of AG (working electrode) is always higher than $-0.1 \text{ V vs. Na}^+/\text{Na}$, revealing that the potential never crosses the threshold of Li plating (Once Li^+ cations become Li-metal, electrostatic shielding will no longer exist).

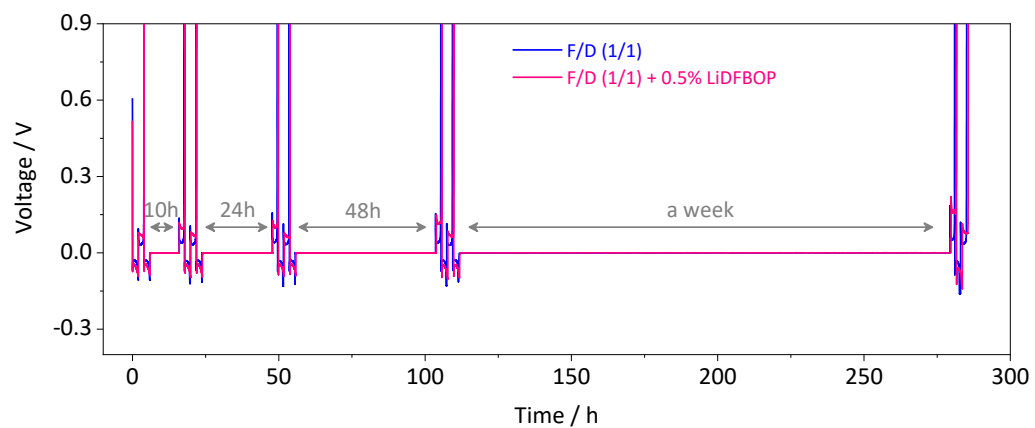


Fig. S10 Voltage profiles of Na plating/stripping on AG operated in F/D (1/1) and F/D (1/1) + 0.5% LiDFBOP at 0.5 mA cm^{-2} and 1 mAh cm^{-2} during calendar ageing tests.

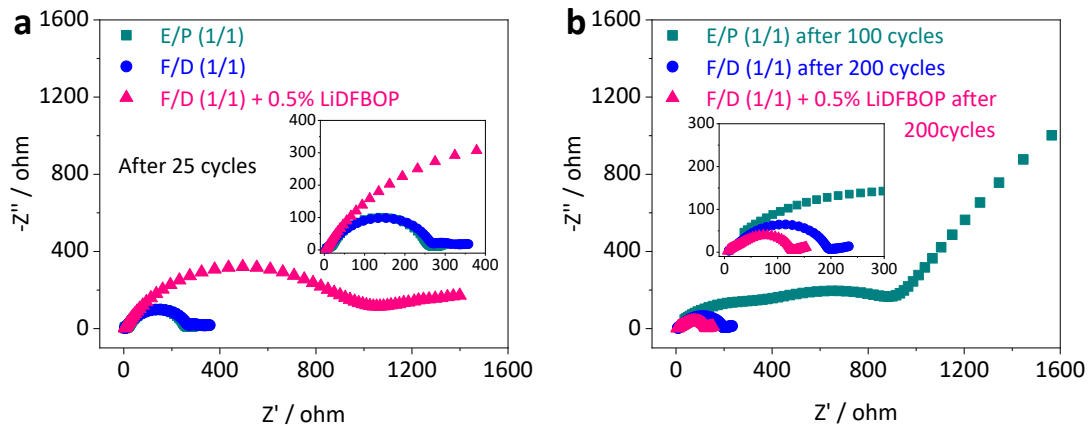


Fig. S11 Electrochemical impedance spectra (EIS) of Na||Na symmetric cells operated in E/P (1/1), F/D (1/1) and F/D (1/1) + 0.5% LiDFBOP after (a) 25 and (b) 200 (100 cycles for E/P (1/1)) cycles.

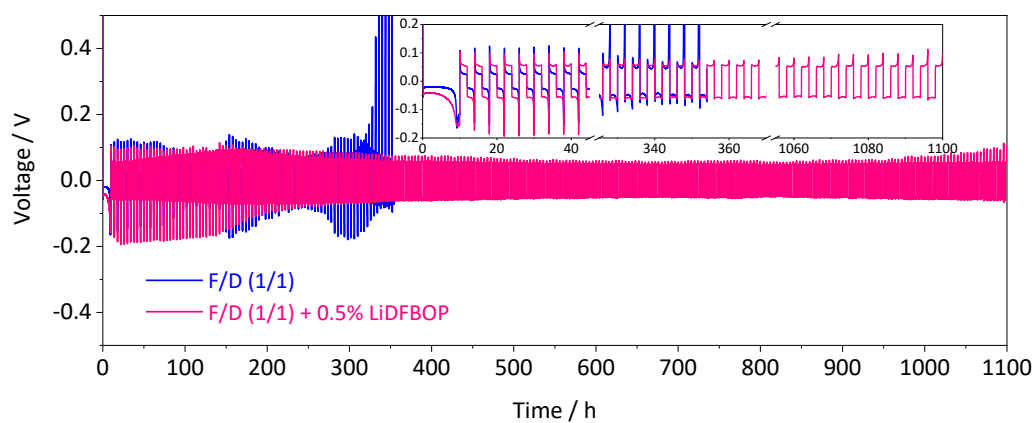


Fig. S12 Cycling performance of Na||Na@AG quasi-symmetric cells operated in F/D (1/1) and F/D (1/1) + 0.5% LiDFBOP at 0.5 mA cm^{-2} and 1 mAh cm^{-2} . Na@AG electrode is prepared by plating 5 mAh cm^{-2} Na on AG substrate under the current density of 0.5 mA cm^{-2} .

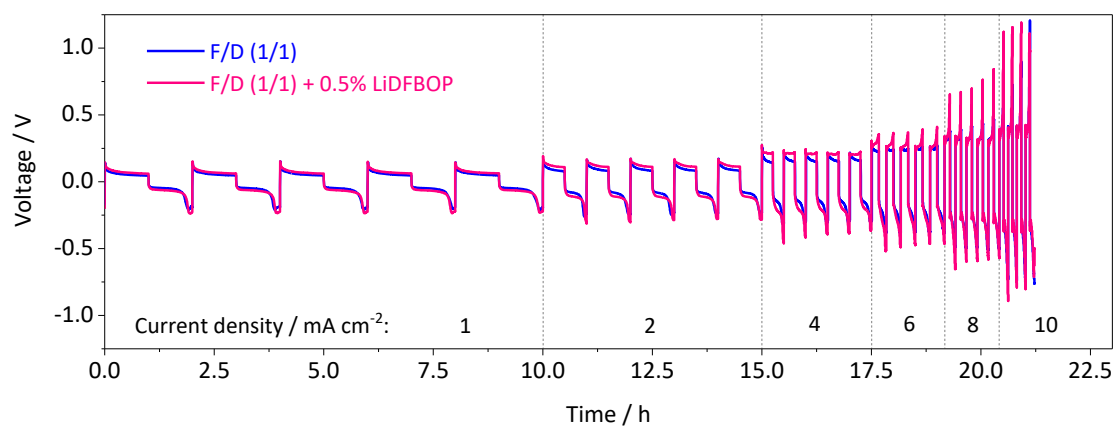


Fig. S13 Rate performance of Na||Na@AG quasi-symmetric cells operated in F/D (1/1) and F/D (1/1) + 0.5% LiDFBOP from 1 mA cm⁻² to 10 mA cm⁻² with a fixed capacity of 1 mAh cm⁻². Na@AG electrode is prepared by plating 5 mAh cm⁻² Na on AG substrate under the current density of 0.5 mA cm⁻².

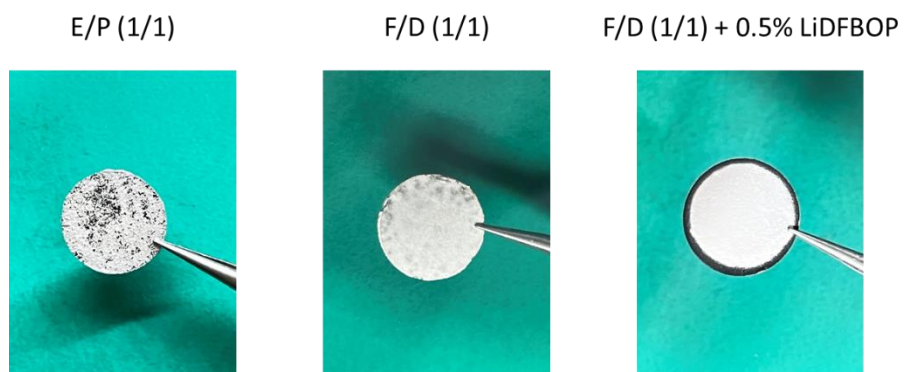


Fig. S14 Optical photos of Na electrodeposits on AG in E/P (1/1), F/D (1/1) and F/D (1/1) + 0.5% LiDFBOP at 0.5 mA cm^{-2} and 2 mAh cm^{-2} .

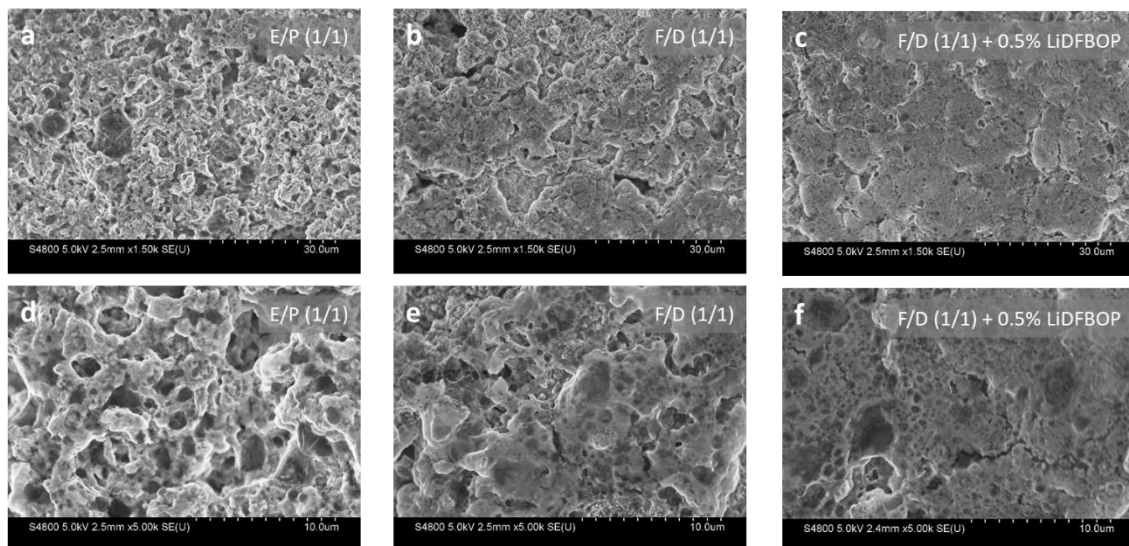


Fig. S15 SEM images of Na electrodes after 20 cycles of Na plating/stripping in Na||AG cells operated in (a, d) E/P (1/1), (b, e) F/D (1/1) and (c, f) F/D (1/1) + 0.5% LiDFBOP.

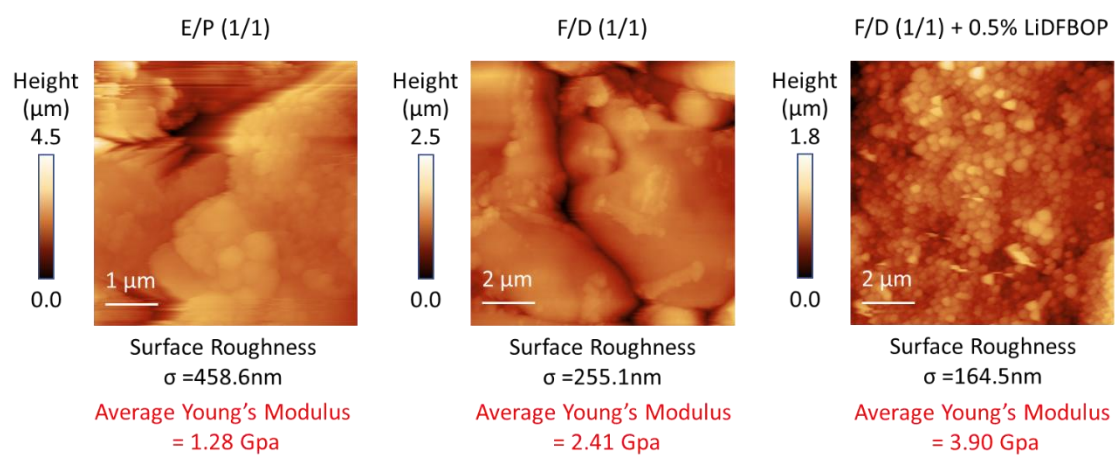


Fig. S16 AFM surface topography and Young's modulus analysis of Na electrodeposits on AG in E/P (1/1), F/D (1/1) and F/D (1/1) + 0.5% LiDFBOP at 0.5 mA cm^{-2} and 2 mAh cm^{-2} .

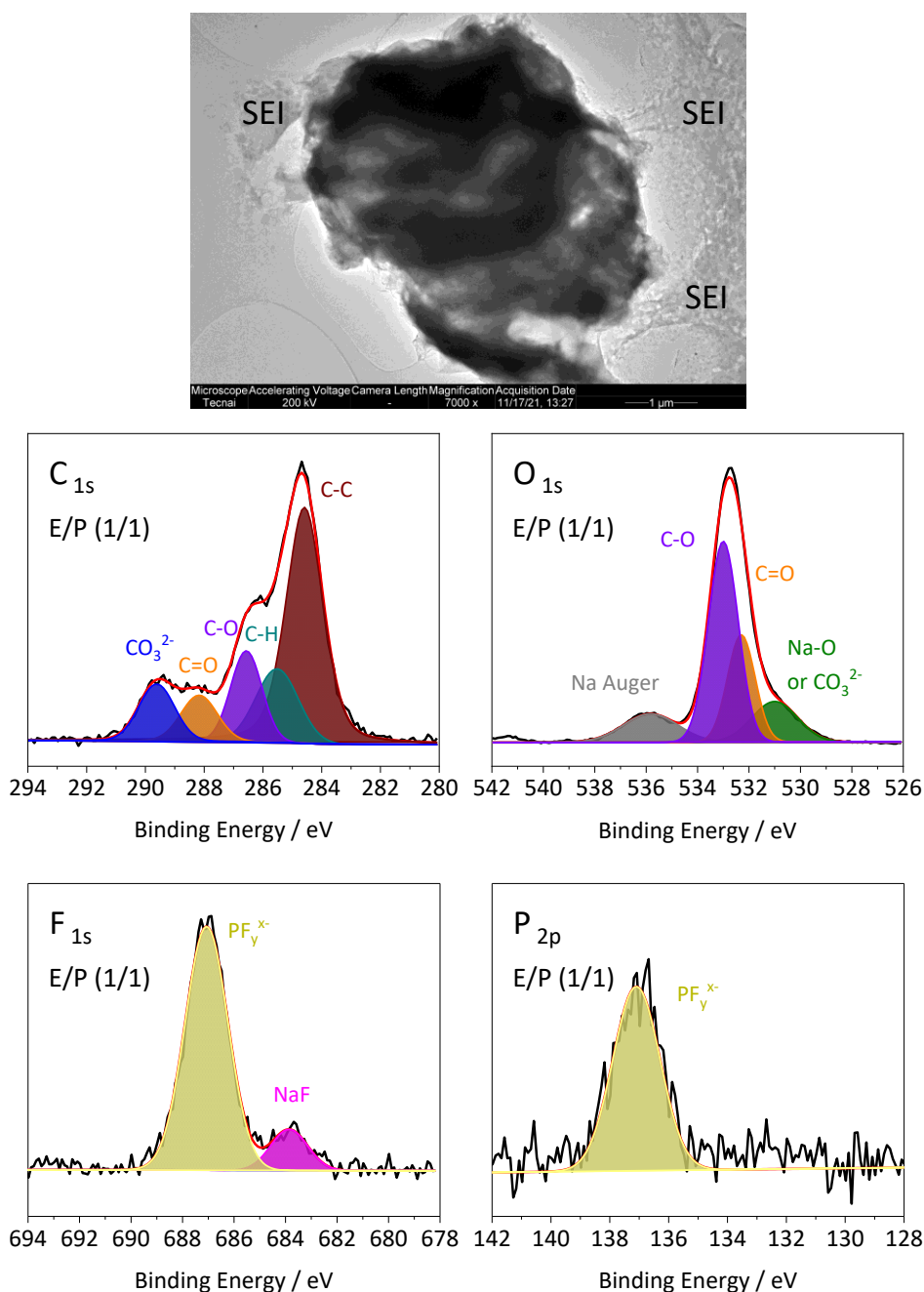


Fig. S17 TEM image and C 1s, O 1s, F 1s and P 2p XPS patterns of AG substrate after repeated Na plating/stripping in E/P (1/1).

After Na plating/stripping in E/P (1/1), the SEI on AG substrate mainly consists of C-O, C=O and CO₃²⁻ species originated from the decompositions of carbonate solvents, while the beneficial species (such as Na-O and NaF) are lacking. Such SEI is electrochemically unstable and mechanically fragile, which can be reflected by a lot of detected decompositions of NaPF₆ (PF_y^{x-}) as well as thick, broken and loose SEI observed in TEM image (The breakage of SEI may be caused by ultrasonic treatment).

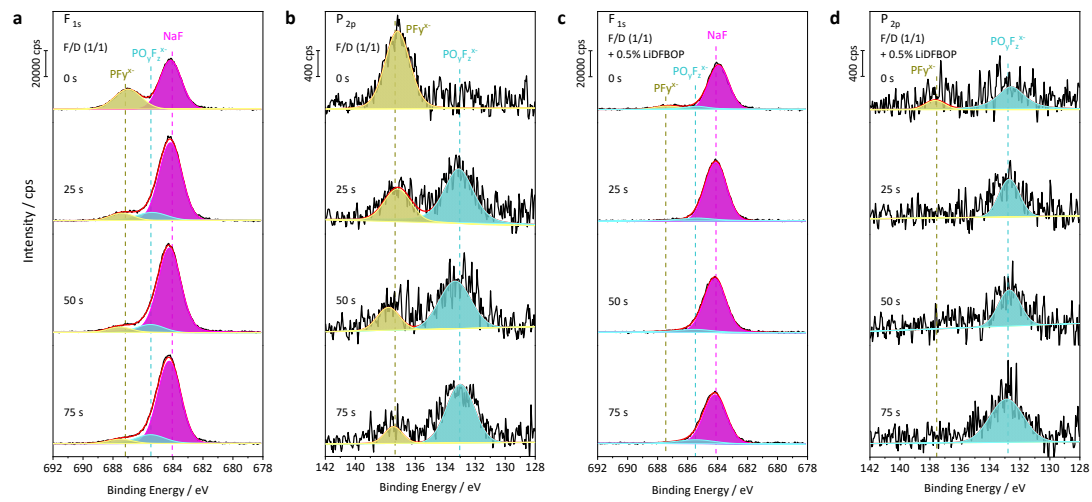


Fig. S18 F 1s and P 2p XPS patterns with various durations of Ar^+ sputtering for AG substrate after repeated Na plating/stripping in (a, b) F/D (1/1) and (c, d) F/D (1/1) + 0.5% LiDFBOP.

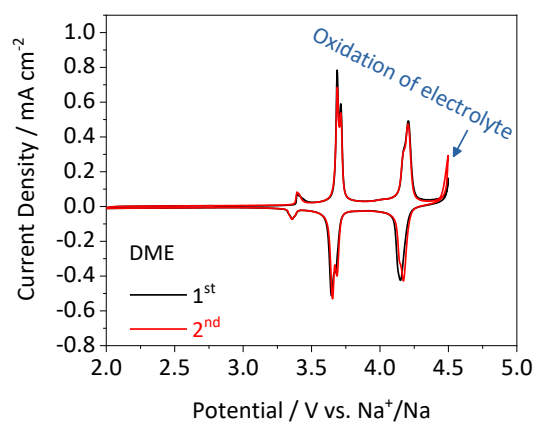


Fig. S19 CV curves of $\text{Na}_3\text{V}_2(\text{PO}_4)_2\text{F}_3$ operated with DME (1 M NaPF_6 in DME) in the three-electrode device at a scan rate of 0.1 mV s^{-1} .

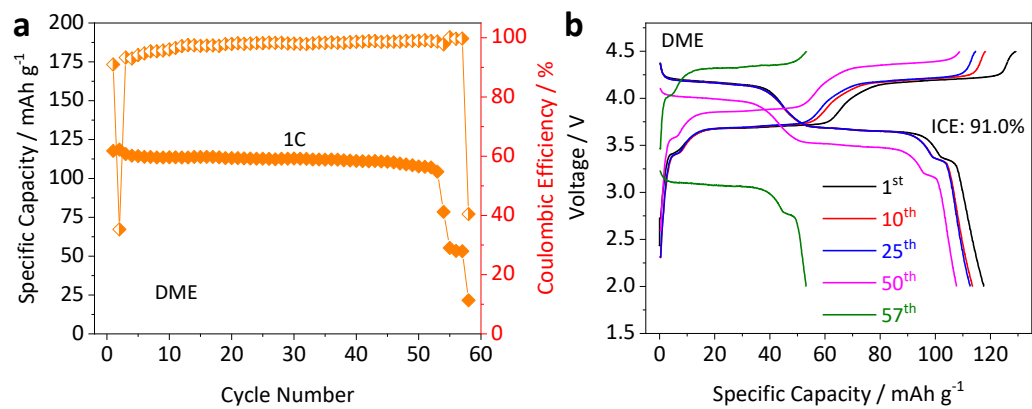


Fig. S20 (a) Cycling performance of Na||Na₃V₂(PO₄)₂F₃ half cell operated in DME at 1 C, and corresponding (b) charge/discharge curves (ICE = initial coulombic efficiency).

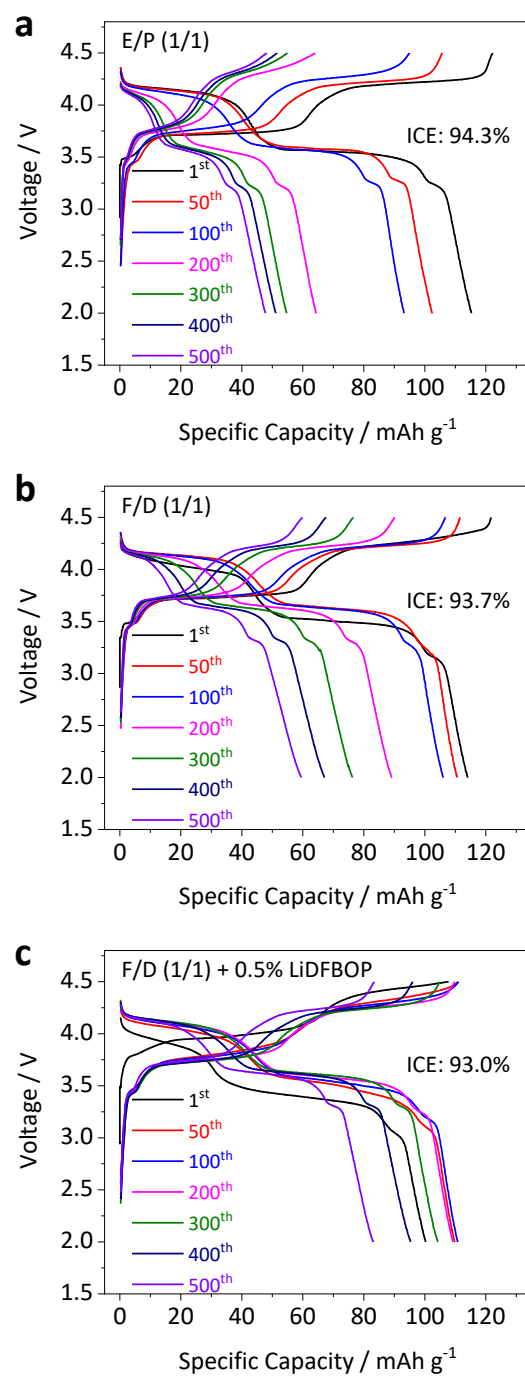


Fig. S21 Charge/discharge curves of Na||Na₃V₂(PO₄)₂F₃ half cells performed in (a) E/P (1/1), (b) F/D (1/1) and (c) F/D (1/1) + 0.5% LiDFBOP at 1 C.

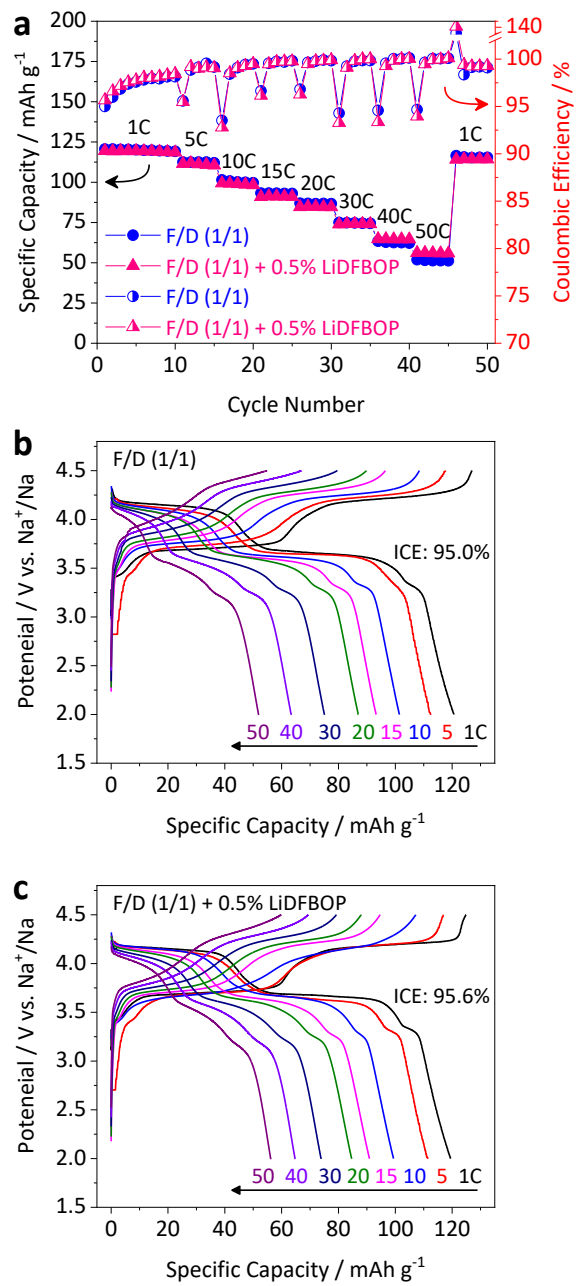


Fig. S22 (a) Rate capabilities of Na₃V₂(PO₄)₂F₃ cathode operated with F/D (1/1) and F/D (1/1) + 0.5% LiDFBOP in three-electrode devices, and corresponding (b, c) charge/discharge curves at different rates.

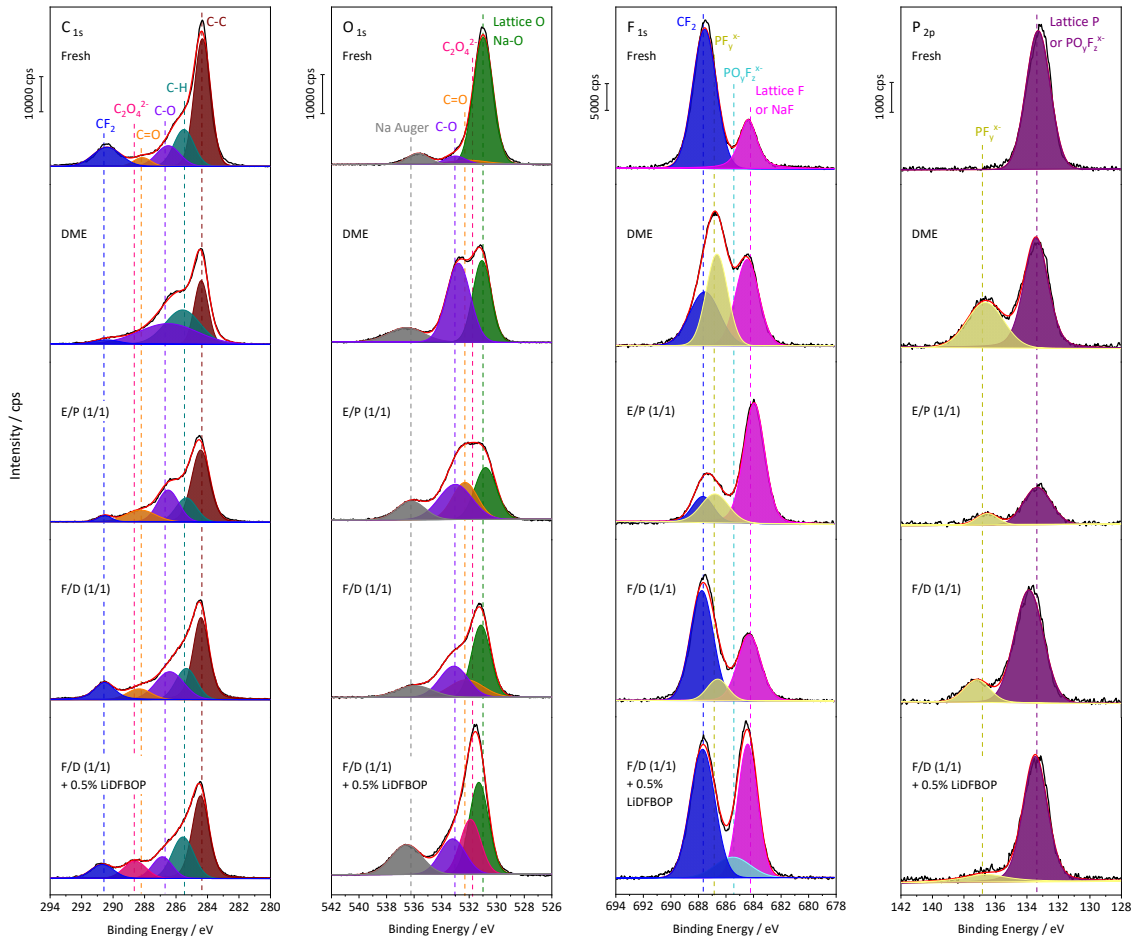


Fig. S23 C 1s, O 1s, F 1s and P 2p XPS patterns of fresh $\text{Na}_3\text{V}_2(\text{PO}_4)_2\text{F}_3$ cathode and those cycled in DME, E/P (1/1), F/D (1/1) and F/D (1/1) + 0.5% LiDFBOP.

The emergent of $\text{C}_2\text{O}_4^{2-}$ species on cycled $\text{Na}_3\text{V}_2(\text{PO}_4)_2\text{F}_3$ cathode in F/D (1/1) + 0.5% LiDFBOP confirms the contribution of DFBOP⁻ on forming CEI, which more effectively inhibits the decompositions of electrolyte (see less PF_y^x from decompositions of NaPF_6 as well as less C-O and C=O from decompositions of solvents) than those in other electrolytes. Moreover, stronger signals of CF_2 from PVdF, C-C from super P, and lattice O, F, P from $\text{Na}_3\text{V}_2(\text{PO}_4)_2\text{F}_3$ further demonstrate this DFBOP⁻-derived CEI is thinner than the others.

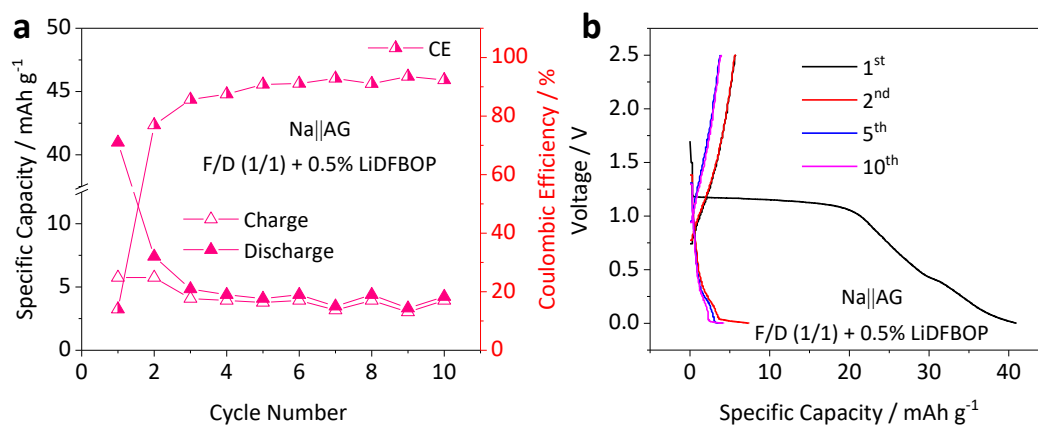


Fig. S24 (a) Cycling performance of the Na||AG cell operated in the voltage range of 0-2.5 V with F/D (1/1) + 0.5% LiDFBOP at the current density of 0.77 mA cm⁻² (equal to the applied current density of Na||Na₃V₂(PO₄)₂F₃ full cell), and corresponding (b) charge/discharge curves.

Given the inability of Na⁺ insertion into graphite layers in carbonate-based electrolyte, AG only delivers a low reversible capacity of around 5 mAh g⁻¹ in F/D (1/1) + 0.5% LiDFBOP. In addition, the mass loading of AG (about 0.8 mg cm⁻²) is much lower than Na₃V₂(PO₄)₂F₃ cathode (about 6 mg cm⁻²). Therefore, the capacity contribution of AG substrate to the total capacity of Na||Na₃V₂(PO₄)₂F₃ full cell is negligible (lower than 1 mAh g⁻¹).

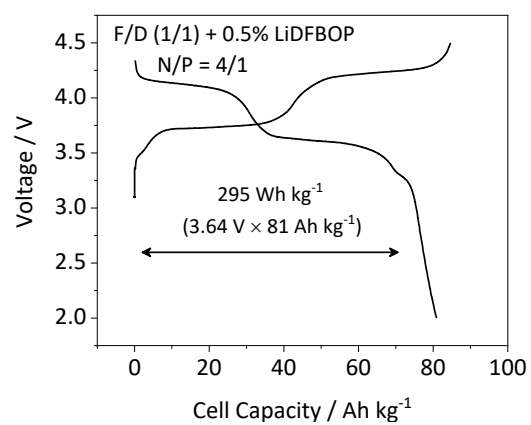


Fig. S25 Energy density of Na||Na₃V₂(PO₄)₂F₃ full cell (N/P = 4/1) operated in F/D (1/1) + 0.5% LiDFBOP at 1 C (The cell capacity is based on total mass of cathode and anode active materials).

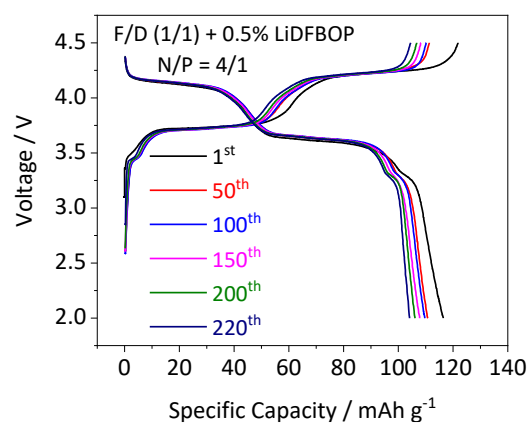


Fig. S26 Charge/discharge curves of Na||Na₃V₂(PO₄)₂F₃ full cell (N/P = 4/1) operated in F/D (1/1) + 0.5% LiDFBOP at 1 C.

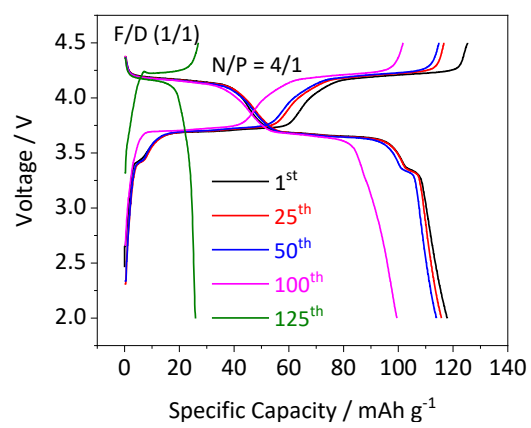


Fig. S27 Charge/discharge curves of Na||Na₃V₂(PO₄)₂F₃ full cell (N/P = 4/1) operated with F/D (1/1) at 1 C.

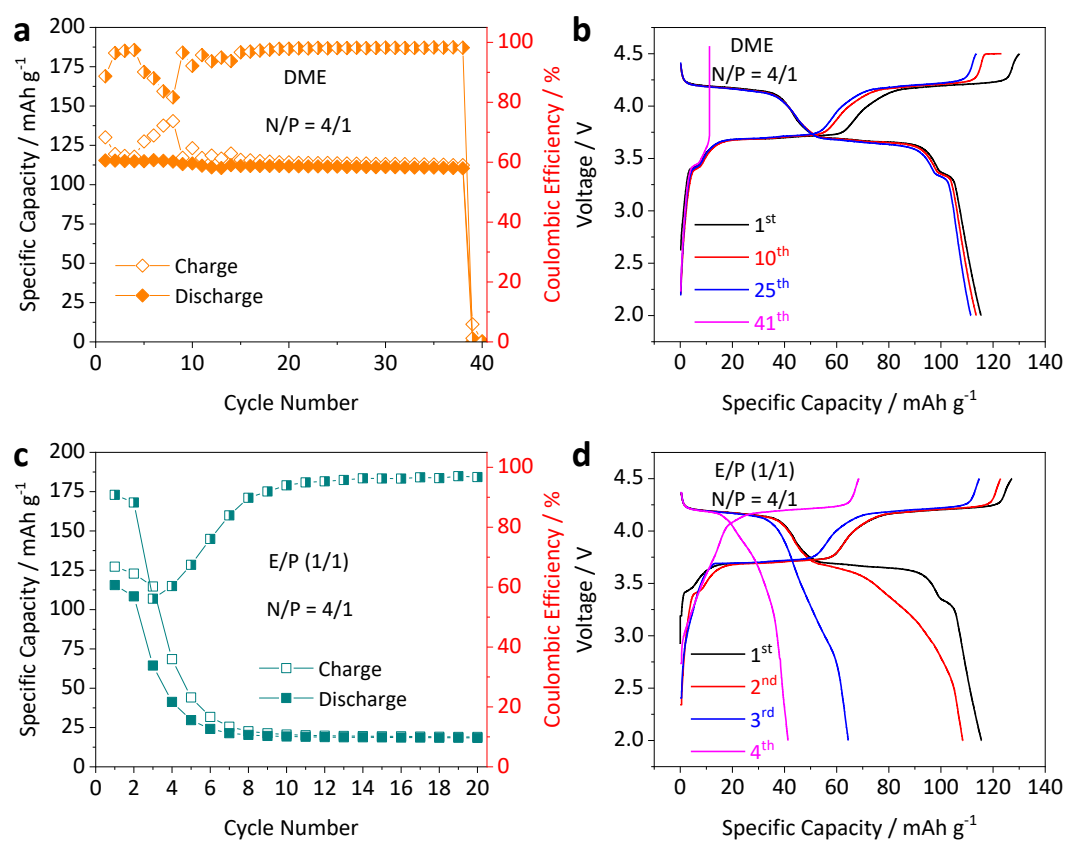


Fig. S28 Cycling performance and corresponding charge/discharge curves of Na||Na₃V₂(PO₄)₂F₃ full cells (N/P = 4/1) operated with (a, b) DME and (c, d) E/P (1/1) at 1 C.

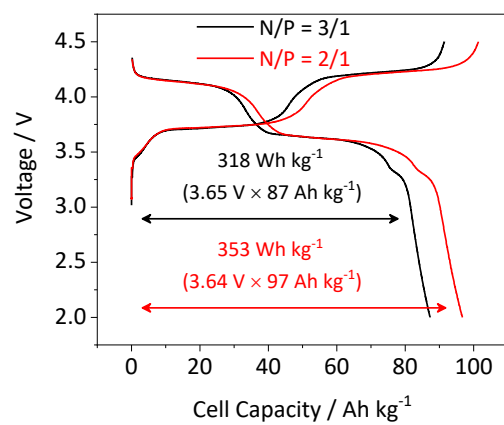


Fig. S29 Energy densities of Na||Na₃V₂(PO₄)₂F₃ full cells with N/P ratios of 3/1 and 2/1 operated in F/D (1/1) + 0.5% LiDFBOP at 1 C (The cell capacity is based on total mass of cathode and anode active materials).

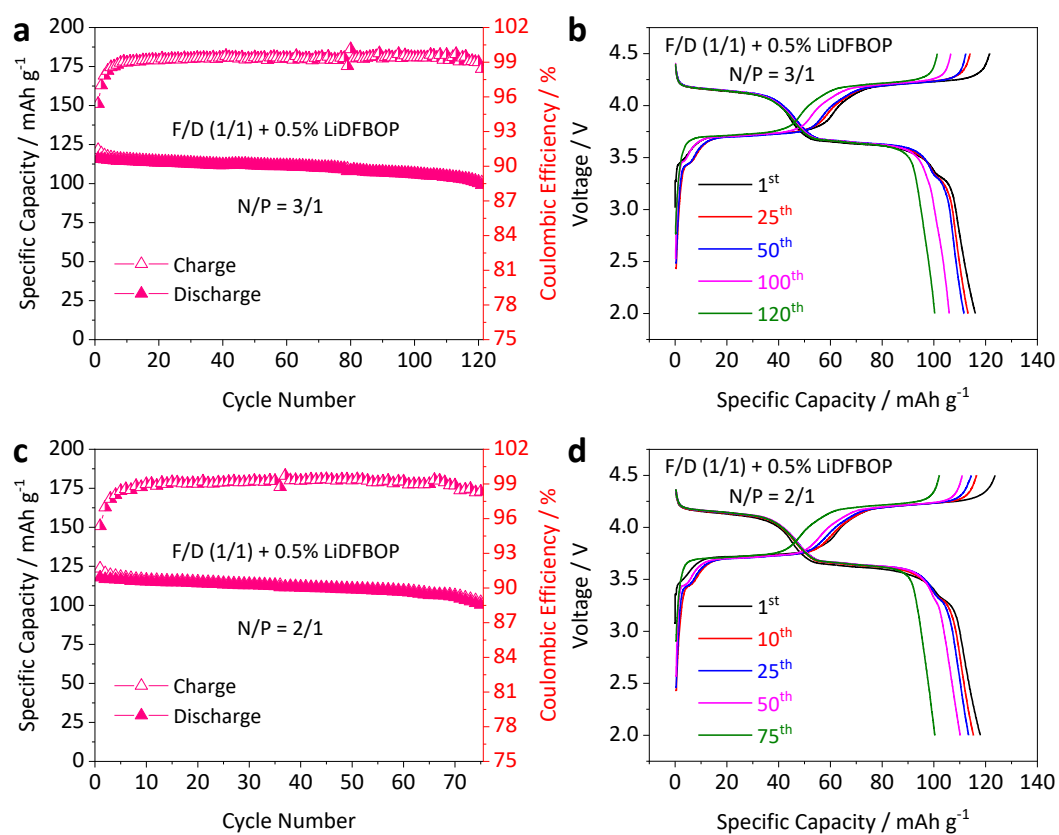


Fig. S30 Cycling performance and corresponding charge/discharge curves of Na||Na₃V₂(PO₄)₂F₃ full cells with N/P ratios of (a, b) 3/1 and (c, d) 2/1 operated in F/D (1/1) + 0.5% LiDFBOP at 1 C.

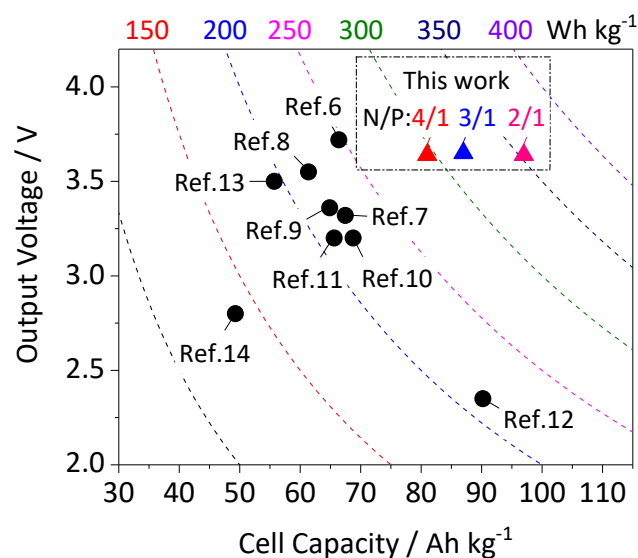


Fig. S31 Energy densities (based on total mass of cathode and anode active materials) of our Na||Na₃V₂(PO₄)₂F₃ SMBs with N/P ratios of 4/1, 3/1 and 2/1, together with those obtained in SIBs, which involve hard carbon (HC)||Na₃V₂(PO₄)₂O₂F,⁶ HC||Na_{0.61}[Mn_{0.27}Fe_{0.34}Ti_{0.39}]O₂,⁷ HC||[Na_{0.67}Zn_{0.05}]Ni_{0.18}Cu_{0.1}Mn_{0.67}O₂,⁸ HC||Na_{0.7}Li_{0.06}Mg_{0.06}Ni_{0.22}Mn_{0.67}O₂,⁹ Na₂Ti₃O₇||VOPO₄,¹⁰ HC||Na_{0.9}[Cu_{0.22}Fe_{0.30}Mn_{0.48}]O₂,¹¹ HC||Na_{2/3}Ni_{1/3}Mn_{2/3}O₂,¹² HC||Na_{7/9}Cu_{2/9}Fe_{1/9}Mn_{2/3}O₂,¹³ Na_{0.8}Ni_{0.4}Ti_{0.6}O₂||Na_{0.8}Ni_{0.4}Ti_{0.6}O₂.¹⁴

Table S1 Comparisons of average Na plating/stripping CEs obtained in our optimized electrolyte system and those in other carbonate-based electrolytes.

Ref.	Electrolyte formula	Current; Capacity	CE/Life-span	Substrate
This work	1 M NaPF₆ in FEC/DEC (1/1 by volume) + 0.5 wt.% LiDFBOP	0.5 mA cm⁻²; 1 mAh cm⁻²	98.6%/300 cycles	AG
15	1 M NaTFSI in FEC	0.25 mA cm ⁻² ; 0.5 mAh cm ⁻²	<96%/100 cycles	Al
16	1 M NaPF ₆ in FEC/PC/HFE (3/3/4 by volume)	0.5 mA cm ⁻² ; 0.5 mAh cm ⁻²	90.3%/100 cycles	Cu
16	1 M NaPF ₆ in FEC/PC/HFE (3/3/4 by volume) + 5 vol.% PFMP	0.5 mA cm ⁻² ; 0.5 mAh cm ⁻²	94.2%/100 cycles	Cu
17	0.8 M NaPF ₆ in FEC/EMC/HFE (3/3/4 by volume)	1 mA cm ⁻² ; 2 mAh cm ⁻² 0.5 mA cm ⁻² ; 0.5 mAh cm ⁻²	95.3%/100 cycles 93.1%/250 cycles	Cu
18	1 M NaTFSI in FEC + 0.75 wt.% NaAsF ₆	0.1 mA cm ⁻² ; 0.5 mAh cm ⁻²	<97%/400 cycles	Al
19	1 M NaFSI in EC/PC (1/1 by volume) + 1 wt.% FEC	0.28 mA cm ⁻² ; 0.56 mAh cm ⁻²	~37%/100 cycles	Cu
19	1 M NaFSI in FEC	0.28 mA cm ⁻² ; 0.56 mAh cm ⁻²	~94%/100 cycles	Cu
20	1 M NaClO ₄ in PC + 5 wt.% FEC	1 mA cm ⁻² ; 1 mAh cm ⁻²	<98%/190 cycles	3D Na ₃ V ₂ (PO ₄) ₃
21	1 M NaClO ₄ in EC/PC (1/1 by volume) + 5 wt.% FEC	1 mA cm ⁻² ; 1 mAh cm ⁻²	<90%/50 cycles	Cu
22	1 M NaClO ₄ in EC/DMC (1/1 by volume) + 5 wt.% FEC	1 mA cm ⁻² ; 1 mAh cm ⁻²	~80%/26 cycles	MOF-coated Cu
23	NaFSI/PC from 10/1 to 1.5/1 (mole ratio)	0.2 mA cm ⁻² ; 0.2 mAh cm ⁻²	<50%/250 cycles	Cu

24

1 M NaPF₆ in EC/DMC
(1/1 by volume)

0.5 mA cm⁻²; 1 mAh cm⁻²

<20%/25 cycles

Cu

Table S2 Comparisons of cycling performance of Na||Na symmetric cells operated with our optimized electrolyte system and those with other carbonate-based electrolytes.

Ref.	Electrolyte formula	Current; Capacity	Life-span
This work	1 M NaPF₆ in FEC/DEC (1/1 by volume) + 0.5 wt.% LiDFBOP	1 mA cm⁻²; 1 mAh cm⁻²	2600 h
15	1 M NaTFSI in FEC	0.25 mA cm ⁻² ; 0.5 mAh cm ⁻²	<500 h
16	1 M NaPF ₆ in FEC/PC/HFE (3/3/4 by volume) + 5 vol.% PFMP	0.5 mA cm ⁻² ; 1 mAh cm ⁻² 1 mA cm ⁻² ; 1 mAh cm ⁻²	1100 h 560 h
17	0.8 M NaPF ₆ in FEC/EMC/HFE (3/3/4 by volume)	1 mA cm ⁻² ; 1 mAh cm ⁻²	<600 h
18	1 M NaTFSI in FEC + 0.75 wt.% NaAsF ₆	0.25 mA cm ⁻² ; 0.5 mAh cm ⁻² 0.5 mA cm ⁻² ; 1 mAh cm ⁻²	550 h 340 h
20	1 M NaClO ₄ in PC + 5 wt.% FEC	1 mA cm ⁻² ; 1 mAh cm ⁻²	200 h
21	1 M NaClO ₄ in EC/PC (1/1 by volume) + 5 wt.% FEC	1 mA cm ⁻² ; 1 mAh cm ⁻²	100 h
25	2 M NaTFSI in TMP/FEC (7/3 by volume)	1 mA cm ⁻² ; 0.5 mAh cm ⁻² 0.3 mA cm ⁻² ; 0.3 mAh cm ⁻²	160 h 1000 h
26	1 M NaClO ₄ in EC/PC (1/1 by volume) + 50 mM SnCl ₂	0.5 mA cm ⁻² ; 1 mAh cm ⁻²	500 h
27	1 M NaClO ₄ in PC + 2 vol.% FEC	0.5 mA cm ⁻² ; 0.5 mAh cm ⁻²	1000 h
28	1 M NaPF ₆ in DME/FEC/HFPM (2/1/2 by volume)	1 mA cm ⁻² ; 1 mAh cm ⁻²	900 h

References

- 1 J. Chen, Y. Peng, Y. Yin, Z. Fang, Y. Cao, Y. Wang, X. Dong and Y. Xia, *Angew. Chem. Int. Ed.*, 2021, **60**, 23858-23862.
- 2 X. Zhang, F. Hao, Y. Cao, Y. Xie, S. Yuan, X. Dong and Y. Xia, *Adv. Funct. Mater.*, 2021, **31**, 2009778.
- 3 H. Ye, C.-Y. Wang, T.-T. Zuo, P.-F. Wang, Y.-X. Yin, Z.-J. Zheng, P. Wang, J. Cheng, F.-F. Cao and Y.-G. Guo, *Nano Energy*, 2018, **48**, 369-376.
- 4 B. D. Adams, J. Zheng, X. Ren, W. Xu and J.-G. Zhang, *Adv. Energy Mater.*, 2018, **8**, 1702097.
- 5 P. Li, C. Li, Y. Yang, C. Zhang, R. Wang, Y. Liu, Y. Wang, J. Luo, X. Dong and Y. Xia, *Research*, 2019, **2019**, 7481319.
- 6 H.-J. Liang, Z.-Y. Gu, X.-X. Zhao, J.-Z. Guo, J.-L. Yang, W.-H. Li, B. Li, Z.-M. Liu, W.-L. Li and X.-L. Wu, *Angew. Chem. Int. Ed.*, 2021, **60**, 26837-26846.
- 7 S. Xu, Y. Wang, L. Ben, Y. Lyu, N. Song, Z. Yang, Y. Li, L. Mu, H.-T. Yang, L. Gu, Y.-S. Hu, H. Li, Z.-H. Cheng, L. Chen and X. Huang, *Adv. Energy Mater.*, 2015, **5**, 1501156.
- 8 B. Peng, Y. Chen, F. Wang, Z. Sun, L. Zhao, X. Zhang, W. Wang and G. Zhang, *Adv. Mater.*, 2022, **34**, 2103210.
- 9 Y.-N. Zhou, P.-F. Wang, Y.-B. Niu, Q. Li, X. Yu, Y.-X. Yin, S. Xu and Y. G. Guo, *Nano Energy*, 2019, **55**, 143-150.
- 10 H. Li, L. Peng, Y. Zhu, D. Chen, X. Zhang and G. Yu, *Energy Environ. Sci.*, 2016, **9**, 3399-3405.
- 11 L. Mu, S. Xu, Y. Li, Y.-S. Hu, H. Li, L. Chen and X. Huang, *Adv. Mater.*, 2015, **27**, 6928.
- 12 Y. Liu, Q. Shen, X. Zhao, J. Zhang, X. Liu, T. Wang, N. Zhang, L. Jiao, J. Chen and L.-Z. Fan, *Adv. Funct. Mater.*, 2019, **30**, 1907837.
- 13 Y. Li, Z. Yang, S. Xu, L. Mu, L. Gu, Y.-S. Hu, H. Li and L. Chen, *Adv. Sci.*, 2015, **2**, 1500031.
- 14 S. Guo, H. Yu, P. Liu, Y. Ren, T. Zhang, M. Chen, M. Ishida and H. Zhou, *Energy Environ. Sci.*, 2015, **8**, 1237-1244.
- 15 S. Wang, Y. Jie, Z. Sun, W. Cai, Y. Chen, F. Huang, Y. Liu, X. Li, R. Du, R. Cao, G. Zhang and S. Jiao, *ACS Appl. Energy Mater.*, 2020, **3**, 8688-8694.
- 16 X. Zheng, Z. Gu, X. Liu, Z. Wang, J. Wen, X. Wu, W. Luo and Y. Huang, *Energy Environ. Sci.*, 2020, **13**, 1788-1798.
- 17 X. Zheng, Z. Gu, J. Fu, H. Wang, X. Ye, L. Huang, X. Liu, X. Wu, W. Luo and Y. Huang, *Energy*

Environ. Sci., 2021, **14**, 4936-4947.

18 S. Wang, W. Cai, Z. Sun, F. Huang, Y. Jie, Y. Liu, Y. Chen, B. Peng, R. Cao, G. Zhang and S. Jiao, *Chem. Commun.*, 2019, **55**, 14375-14378.

19 Y. Lee, J. Lee, J. Lee, K. Kim, A. Cha, S. Kang, T. Wi, S. J. Kang, H.-W. Lee and N.-S. Choi, *ACS Appl. Mater. Interfaces*, 2018, **10**, 15270-15280.

20 M. Guo, H. Dou, W. Zhao, X. Zhao, B. Wan, J. Wang, Y. Yan, X. Wang, Z.-F. Ma and X. Yang, *Nano Energy*, 2020, **70**, 104479.

21 M. Han, C. Zhu, T. Ma, Z. Pan, Z. Tao and J. Chen, *Chem. Commun.*, 2018, **54**, 2381-2384.

22 J. Qian, Y. Li, M. Zhang, R. Luo, F. Wang, Y. Ye, Y. Xing, W. Li, W. Qu, L. Wang, L. Li, Y. Li, F. Wu and R. Chen, *Nano Energy*, 2019, **60**, 866-874.

23 R. Cao, K. Mishra, X. Li, J. Qian, M. H. Engelhard, M. E. Bowden, K. S. Han, K. T. Mueller, W. A. Henderson and J.-G. Zhang, *Nano Energy*, 2016, **30**, 825-830.

24 Z. W. Seh, J. Sun, Y. Sun and Y. Cui, *ACS Cent. Sci.*, 2015, **1**, 449-455.

25 J. Wu, J. Liu, Z. Lu, K. Lin, Y.-Q. Lyu, B. Li, F. Ciucci and J.-K. Kim, *Energy Storage Mater.*, 2019, **23**, 8-16.

26 X. Zheng, H. Fu, C. Hu, H. Xu, Y. Huang, J. Wen, H. Sun, W. Luo and Y. Huang, *J. Phys. Chem. Lett.*, 2019, **10**, 707-714.

27 Y. Xiang, G. Zheng, Z. Liang, Y. Jin, X. Liu, S. Chen, K. Zhou, J. Zhu, M. Lin, H. He, J. Wan, S. Yu, G. Zhong, R. Fu, Y. Li and Y. Yang, *Nat. Nanotechnol.*, 2020, **15**, 883-890.

28 Q. Yi, Y. Lu, X. Sun, H. Zhang, H. Yu and C. Sun, *ACS Appl. Mater. Interfaces*, 2019, **11**, 46965-46972.